

A $f(R)$ -gravity model of the Sunyaev-Zeldovich profile of the Coma cluster compatible with *Planck* data

I. De Martino¹

¹*Department of Theoretical Physics and History of Science, University of the Basque Country UPV/EHU, Faculty of Science and Technology, Barrio Sarriena s/n, 48940 Leioa, Spain; e-mail address: ivan.demartino1983@gmail.com*

In the weak field limit, analytic $f(R)$ models of gravity introduce a Yukawa-like correction to the Newtonian gravitational potential. These models have been widely tested at galactic scales and provide an alternative explanation to the dynamics of galaxies without Dark Matter. We study if the temperature anisotropies due to the thermal Sunyaev-Zeldovich effect are compatible with these Extended Theories of Gravity. We assume that the gas is in hydrostatic equilibrium within the modified Newtonian potential and it is well described by a polytropic equation of state. We particularize the model for the Coma cluster and the predicted anisotropies are compared with those measured in the foreground cleaned maps obtained using the Planck Nominal maps released in 2013. We show that the computed $f(R)$ pressure profile fits the data giving rise to competitive constraints of the Yukawa scale length $L = (2.19 \pm 1.02)$ Mpc, and of the deviation parameter $\delta = -0.48 \pm 0.22$. Those are currently the tightest constraints at galaxy cluster scale, and support the idea that Extended Theories of Gravity provide an alternative explanation to the dynamics of self-gravitating systems without requiring Dark Matter.

PACS numbers: 04.50.Kd, 95.30.Sf, 95.35.+d, 98.65.Cw

I. INTRODUCTION.

Astrophysical and cosmological observations clearly indicate that the Universe has entered into a period of accelerated expansion [1–6]. The Λ CDM model accounts for these observations by requiring two new energy densities: a Dark Matter (DM) component, characterized by a small temperature, interacting only gravitationally with the other energy components and a cosmological constant Λ , equivalent to a perfect fluid with negative pressure: $p = w\rho$ with an equation of state parameter $w = -1$. To explain the current period of accelerated expansion only $w \leq -1/3$ is required. This negative pressure fluid is named Dark Energy (DE). The current values of the energy densities are $\Omega_{DM} \simeq 0.26$ and $\Omega_{\Lambda} \simeq 0.68$, in units of the critical density, and of the equation of state parameter $w = -1.019^{+0.075}_{-0.080}$, compatible with a cosmological constant [5]. Although the effects of DM and DE on large scale are very well constrained, the lack of evidence of counterparts at the particle level has been interpreted as a break on General Relativity (GR) at galactic, extragalactic and cosmological scales and alternative models to GR have been proposed.

Generically, Extended Theories of Gravity (ETGs) generalize the Hilbert-Einstein Lagrangian by including higher-order curvature invariants and minimally or non-minimally coupled terms between scalar fields and geometry. The most studied generalization consists in replacing the Ricci scalar R in the Hilbert-Einstein action with a more general function of the curvature $f(R)$ (for comprehensive reviews see [7–12]). Although many $f(R)$ models can be tested with astrophysical and cosmological observations (see [13] and reference therein), the exact functional form of the gravitational action is still unknown. The higher order terms appearing in the La-

grangian can be recast as additional scalar fields by performing a conformal transformation from the Jordan to the Einstein frame [9]. As an example, chameleon $f(R)$ models introduce a scalar field non-minimally coupled to matter, giving rise to the so called fifth force. These models require a screening mechanism to erase the effect of the scalar field in high density environments to evade the constraints imposed by the Solar System dynamics [14, 15]. Many efforts have been devoted to test these models from astrophysical to cosmological scales [16–23]. For instance, an upper bound on the background amplitude of the chameleon field has been found by studying the gravitational interaction on the outskirts of galaxy clusters [25–27]. At the scale of cluster of galaxies, [24] demonstrated the existence of a degeneracy between the baryonic processes and the underlying theory of gravity. Although it is always possible to transform the model from the Jordan to the Einstein frame and vice-versa since they are conformally equivalent, nothing can be said *a priori* about their physical equivalence that must be studied for each specific case [12, 28, 29].

Alternatively, one could make the whole analysis in the Jordan frame and consider the additional degrees of freedom introduced by the theory of gravity as “free parameters” that must be constrained using data. Thus, those parameters are expected to acquire different values at different scales in order to pass the Solar system constraints. For instance, analytic $f(R)$ models, those expandable in Taylor series around a fixed point R_0 , i.e.,

$$f(R) = \sum_n \frac{f^n(R_0)}{n!} (R - R_0)^n \simeq f_0 + f'_0 R + \frac{f''_0}{2} R^2 + \dots \quad (1)$$

give rise to Yukawa-like corrections of the gravitational

potential in the Newtonian limit [29, 30]

$$\Phi_{grav}(r) = -\frac{GM}{r} \left(\frac{1 + \delta e^{-\frac{r}{L}}}{1 + \delta} \right), \quad (2)$$

where δ quantifies the deviation from GR at zero order and L is an extra gravitational scale length of the self-gravitating object [12]. This new gravitational scale is strictly related to the theory: $f(R)$ gravity is a fourth-order theory and its extra degrees of freedom give rise, in the weak field limit, to a new characteristic scale length (see [31] for the description of the general paradigm on $(2k+2)$ -order theories of gravity). Those two parameters are related to the coefficients in the Taylor expansion, eq. (1), by the relations: $\delta = f'_0 - 1$ and $L = [-6f''_0 f'_0]^{1/2}$ (see Sect. II for a more detailed discussion). Analytic $f(R)$ models have been shown to evade the Solar System constraints [30, 32–35] and to correctly describe the collapse of self-gravitating systems [36], the emission of gravitational waves [33, 37, 38] and the dynamics of elliptical and spiral galaxies without requiring DM [39, 40]. Nevertheless, they are poorly tested at galaxy cluster scale. At such scale, analytic $f(R)$ models provide a good fit to the mass profile of 12 X-ray clusters without requiring a DM halo [41]. An equally attractive test is given by the pressure profile of clusters derived from the Cosmic Microwave Background (CMB) temperature anisotropies generated by the thermal Sunyaev-Zeldovich (TSZ) effect [42]. An upper bound on the parameters of eq. (2) was determined using a reconstructed map of CMB temperature fluctuations, and computing SZ profiles averaged over a sample of 579 galaxy clusters [43]. This led to the bounds $\delta < -0.1$ and $L < 19\text{Mpc}$ at the 95% confidence level (CL).

In this paper we demonstrate that the SZ profiles of clusters agree with the observed profiles when their Intra Cluster gas is in hydrostatic equilibrium within the potential in eq. (2). There is no need to introduce a dominant DM component. We particularize our analysis for the Coma cluster since is located close to the galactic pole where the foreground emission is comparatively low. We use *Planck* 2013 Nominal maps to measure its SZ profile and constrain the parameters (δ, L) of the modified gravitational potential. We assume Coma to be spherically symmetric and the Intra Cluster gas to be in hydrostatic equilibrium. These are good approximations to describe the gas distribution and its dynamical state in the intermediate regions where the non-thermal pressure is expected to be sub-dominant [25, 26, 44]. The outline of the paper is as follows: in Sec. II, we briefly summarize the weak field limit of analytic $f(R)$ -gravity and we discuss the modified gravitational potential limit at small and large scales, in Sec. III, we describe the SZ effect and the model to be tested; in Sec. IV, we describe the main observational features of the Coma cluster and *Planck* 2013 Nominal data, summarizing the procedure used produced foreground cleaned maps, in Sec. V we describe our methodology. Finally, in Sec. VI we present our results and in Sec. VII we summarize our conclusions.

II. YUKAWA-LIKE CORRECTION TO THE NEWTONIAN POTENTIAL FROM THE WEAK FIELD LIMIT OF $f(R)$ -GRAVITY

Our purpose is to test a class of theories of gravity that in the weak field limit gives rise to a Yukawa-like correction of the Newtonian gravitational potential. Let us first consider the action of a $f(R)$ -gravity model in the vacuum [7–12]

$$S = \int d^4x \sqrt{-g} f(R). \quad (3)$$

The corresponding field equations are

$$f'(R)R_{\mu\nu} - \frac{1}{2}f(R)g_{\mu\nu} - f'(R)_{;\mu\nu} + g_{\mu\nu}\square f'(R), \quad (4)$$

and their trace is

$$3\square f'(R) + f'(R)R - 2f(R) = 0. \quad (5)$$

In the post-Newtonian limit, one is interested in describing the motion of the particles beyond the Newtonian approximation by including higher order corrections in the perturbation expansion of the metric. The post-Newtonian limit in a higher order theory of gravity introduces correction terms in the Newtonian gravitational potential. The correcting terms depends on the order of the partial differential equations that describe the gravitational field [28]. For instance, in $f(R) = R^2$ the field equations are fourth order and in the post-Newtonian limit there is a Yukawa-like correction term that modifies the Newtonian potential [45]. This correction also appears in any $f(R)$ -model that can be expanded in Taylor series. To illustrate this point, let us briefly derive the solution of the field equations in the weak field limit for a spherically symmetric matter distribution (a detailed description of the weak field limit in GR can be found in [46], while its analogue in $f(R)$ -gravity was studied in [28, 29]). In this case the metric can be written as

$$ds^2 = g_{00}(ct, r) c^2 dt^2 - g_{11}(ct, r) dr^2 + r^2 d\Omega^2, \quad (6)$$

where $d\Omega^2$ is the solid angle. In order to study the weak field limit, the metric tensor can be written as follows [46]

$$g_{00}(ct, r) = 1 + g_{00}^{(2)}(ct, r) + g_{00}^{(4)}(ct, r), \quad (7)$$

$$g_{11}(ct, r) = -1 + g_{11}^{(2)}(ct, r), \quad (8)$$

$$g_{22}(ct, r) = -r^2, \quad (9)$$

$$g_{33}(ct, r) = -r^2 \sin^2 \theta. \quad (10)$$

These expansions are introduced into the field equations (4) to compute the perturbations at $\mathcal{O}(0)$, $\mathcal{O}(2)$, and $\mathcal{O}(4)$. Particularizing eq. (1) for an analytic $f(R)$ model at order zero one finds the condition

$$\frac{f_0}{2} g_{\mu\nu}^{(0)} = 0, \quad (11)$$

that automatically implies $f_0 = 0$. Thus, the solutions at higher orders will not depend on this parameter. If we now consider the approximation at second order, the vacuum field equations can be re-written as

$$f'_0 r R^{(2)} - 2f'_0 \partial_r g_{tt}^{(2)} + 8f''_0 \partial_r R^{(2)} - f'_0 r \partial_r^2 g_{tt}^{(2)} + f''_0 r R^{(2)} = 0, \quad (12)$$

$$f'_0 r R^{(2)} - 2f'_0 \partial_r g_{rr}^{(2)} + 8f''_0 \partial_r R^{(2)} - f'_0 r \partial_r^2 g_{rr}^{(2)} = 0, \quad (13)$$

$$2f'_0 g_{11}^{(2)} - r[f'_0 r R^{(2)} - f'_0 \partial_r g_{tt}^{(2)} - f'_0 \partial_r g_{rr}^{(2)} + 4f''_0 \partial_r R^{(2)} + 4f''_0 r \partial_r^2 R^{(2)}] = 0, \quad (14)$$

$$f'_0 r R^{(2)} + 6f''_0 [2\partial_r R^{(2)} + r\partial_r^2 R^{(2)}] = 0, \quad (15)$$

$$2g_{11}^{(2)} + r[2\partial_r g_{tt}^{(2)} - rR^{(2)} + 2\partial_r g_{rr}^{(2)} + r\partial_r^2 g_{tt}^{(2)}] = 0. \quad (16)$$

These generic expressions can be particularized for a specific theory selecting the corresponding coefficients f_i in the Taylor expansion of eq. (1). In other words, this system of equations can be re-written for any $f(R)$ -Lagrangian as long as it is expandable in Taylor series. The solution of eqs. (12)-(16) is [29, 30]

$$g_{tt}^{(2)} = \delta_0 - \frac{\Upsilon}{f'_0 r} - \frac{\delta_1(t)e^{-r\sqrt{\xi}}}{3\xi r} + \frac{\delta_2(t)e^{r\sqrt{\xi}}}{6(-\xi)^{3/2}r}, \quad (17)$$

$$g_{rr}^{(2)} = -\frac{\Upsilon}{f'_0 r} + \frac{\delta_1(t)[r\sqrt{\xi} + 1]e^{-r\sqrt{\xi}}}{3\xi r} - \frac{\delta_2(t)[\xi r + \sqrt{\xi}]e^{r\sqrt{\xi}}}{6\xi^2 r}, \quad (18)$$

$$R^{(2)} = \frac{\delta_1(t)e^{-r\sqrt{\xi}}}{r} - \frac{\delta_2(t)\sqrt{\xi}e^{r\sqrt{\xi}}}{2\xi}, \quad (19)$$

where Υ is an arbitrary integration constant, the coefficient $\xi = -\frac{f'_0}{6f''_0}$ has units of $(length)^{-2}$, and f'_0 and f''_0 are the Taylor coefficients of the Lagrangian; δ_0 is dimensionless and the time dependent functions $\delta_1(t)$, $\delta_2(t)$ have dimensions $(length)^{-1}$, $(length)^{-2}$, respectively. Since in the weak field limit $g_{tt} = 1 + 2\phi_{grav} = 1 + g_{tt}^{(2)}$, then $\delta_0 = 0$ and

$$\Phi_{grav} = -\frac{\Upsilon}{2f'_0 r} - \frac{\delta_1(t)e^{-r\sqrt{-\xi}}}{6\xi r} + \frac{\delta_2(t)e^{r\sqrt{-\xi}}}{12(-\xi)^{3/2}r}. \quad (20)$$

When $r \rightarrow \infty$, the potential must go to zero. Imposing this condition yields $\delta_2(t) \equiv 0$. Finally, to restore GR in the limit $f'_0 = 1$ and $f''_0 = 0$, then $\Upsilon = 2GM$. Introducing the notation of $\sqrt{-\xi} = 1/L$, where now L has units of length, $\delta_1 = -\frac{6GM}{L^2} \frac{\delta}{1+\delta}$, and $1 + \delta = f'_0$, the eq. (20) can be rewritten as the modified potential of eq. (2).

A. Small and large scale limits of the modified gravitational potential

The general result of eq. (2) implies that the Newtonian potential describes the gravitational interaction only in the particular case of the Einstein-Hilbert Lagrangian, *i.e.* $f(R) = R$. In other words, the parameters of the Yukawa-like correction, (δ, L) , represent the deviation of the gravitational potential from the standard Newtonian gravity. As it is well known, any high order theory of gravity has to evade the Solar System constraints. Specifically, at small scales ($r \ll L$) the Yukawa term in the gravitational potential is not in contradiction with Solar System observations [35, 47]. In fact, in the GR limit $f'_0 = 1$ and $f''_0 = 0$ and $\delta = f'_0 - 1 = 0$ and $L = \sqrt{-6f''_0/f'_0} = 0$. Thus, from eq. (2), the Newtonian potential is restored and no violation of the Solar System constraints appears. Since there is no general prescription that ensures the physical equivalence of the weak field limit in the Jordan and the Einstein frames [48–50], no conformal transformation was made to read these extra degrees of freedom as some scalar fields [51, 52]. Nevertheless, apart of a possible inadequacy in comparing results from the two frames, one can re-write any $f(R)$ model as a scalar-tensor theory plus a scalar field (ϕ). Then, in the small scale limit the mass of the scalar field, given by $m_\phi^2 = -f'_0/3f''_0 = 2/L^2$, diverges [53]. This divergence corresponds to the well-known chameleon mechanism which requires the scalar field to be suppressed (at small scales) in high density environments [14]. At large scales, the values $f'_0 \neq 1$ and $f''_0 \neq 0$ generate deviations from Newtonian gravity, open the possibility to observationally confirm or rule out these alternative theories of gravity.

Modifications of the Einstein-Hilbert Lagrangian have an effect at all scales. As indicated such modifications have to evade the well established Solar System constraints. At galaxy scales the corrections to the Newtonian gravitational potential can describe systems like spiral and elliptical galaxies, and galaxy clusters without resorting to DM. Detailed analysis at galaxy scales have been carried out [39, 40], there is not a definitive answer on whether the assumptions on the underlying theory of gravity are correct or not. Our purpose is to test such theories using clusters of galaxies, the largest virialized objects in the Universe, to test modified models of gravity at scales intermediate between galactic and cosmological scales. Let us also remark that in the limit $r \gg L$ the gravitational potential is that of a point-like mass $M/(1+\delta)$. In this limit, the dynamics is Newtonian and to explain the structure of self-gravitating systems and the evolution of large scale structure, DM needs to be introduced as in the standard cosmological model.

III. THE SUNYAEV-ZELDOVICH CLUSTER PROFILE IN $f(R)$ -GRAVITY.

Cluster of galaxies are the largest virialized objects in the Universe. Their Intra-Cluster Medium (ICM) reaches temperatures in the range $T_e \sim 1 - 10\text{keV}$. When CMB photons cross the potential wells of clusters, they gain energy via inverse Compton scattering with the hot electrons of the ICM. The CMB temperature anisotropies generated by the Sunyaev-Zeldovich effect (SZ) have two components: the thermal SZ effect (TSZ, [42]) due to the thermal motion of the ICM medium and the kinematic SZ effect (KSZ, [54]) due to the proper motion of the cluster with respect to the isotropic CMB frame. The TSZ is usually expressed in terms of the Comptonization parameter y_c as

$$\begin{aligned} \frac{\Delta T_{TSZ}(\hat{n})}{T_0} &= G(x)y_c = G(x)\frac{k_B\sigma_T}{mc^2} \int_l T_e(l)n_e(l)dl = \\ &= G(\nu)\frac{\sigma_T}{mc^2} \int_l P_e(l)dl. \end{aligned} \quad (21)$$

In this expression T_0 is the current value of the CMB black-body temperature $T_0 = 2.725 \pm 0.002\text{K}$ [55], $G(\nu)$ is the spectral dependence of the TSZ effect, σ_T the Thomson cross section, m_e the electron mass, c the speed of light and k_B the Boltzmann constant. The pressure profile along the line of sight (l.o.s.) $P_e(l)$ is given by $P_e(l) = n_e(l)T_e(l)$, where $n_e(l)$ and $T_e(l)$ are the electron density and electron temperature, respectively. In the non relativistic limit ($T_e \approx \text{few keV}$), $G(\nu) = \tilde{\nu}\coth(\tilde{\nu}/2) - 4$ where $\tilde{\nu} = h\nu/k_B T_e$ is the reduced frequency. To improve the description of the TSZ effect, we included relativistic corrections in the electron temperature up to fourth order ([57–59]).

To compute the pressure profile of eq. (21) in $f(R)$ gravity, we follow the procedure described in [43]. We consider the analytic $f(R)$ model given by eq. (1), and the modified gravitational potential of eq. (2) generalized for an extended spherically symmetric system [41]. Further, the gas is assumed to be in hydrostatic equilibrium within the modified potential well of the galaxy cluster

$$\frac{d\mathbb{P}(r)}{dr} = -\rho(r)\frac{d\Phi_{grav}^{extended}(r)}{dr} \quad (22)$$

and it is well described by a polytropic equation of state

$$\mathbb{P}(r) \propto \rho^\gamma(r) \quad (23)$$

The system of equation is closed with the conservation of the mass

$$\frac{dM(r)}{dr} = 4\pi\rho(r). \quad (24)$$

The density $\rho(r)$ refers to the gas density residing in the modified potential well of the cluster and does not include a DM component. The pressure profile $P(r) = P_c\mathbb{P}(r)$ is given in terms of the two gravitational parameters (δ, L)

characterizing the theory, the polytropic index γ , and the central pressure P_c . The resulting profile will be integrated along the l.o.s. and convolved with the antenna beam of the different *Planck* channels to predict the TSZ temperature fluctuations.

IV. DATA.

We use the *Planck* 2013 Nominal maps¹ to measure the TSZ temperature anisotropies induced by the Coma cluster. *Planck* maps were originally released in a Healpix format with resolution $N_{side} = 2048$ [60].

A. The Coma Cluster.

The nearby Coma Cluster is one of the best studied clusters of galaxies because of its richness, degree of symmetry and location near the galactic pole. It is located at redshift $z = 0.023$. Its X-ray luminosity and temperature are $L_X \sim 7.77 \times 10^{44} \text{erg/s}$ in the $[0.1 - 2.4]\text{keV}$ band [61] and $T_e = 6.9_{-0.8}^{+0.1}\text{keV}$ [56]. Recently, the Planck Collaboration [62] determined that the angular size subtended by the r_{500} scale was $\theta_{500} = 48 \pm 1 \text{arcmin}$, corresponding to $r_{500} \sim 1.314\text{Mpc}$ in the concordance model; the associated mass is $M_{500} \sim 6 \times 10^{14}M_\odot$. Substructure, cooling processes in the cluster core and departure from the spherical symmetry have been shown to exist [63–71]. All these components affect the inner- and outer-most regions of the cluster, but in the intermediate regions the assumptions of hydrostatic equilibrium and spherical symmetry hold [25–27, 44]. Therefore, we will restrict our analysis to this intermediate region.

B. Foreground cleaned *Planck* Nominal Maps.

Planck Nominal maps were released in 2013. In addition to the intrinsic CMB temperature anisotropies, SZ effect and instrumental noise, they contain foreground emissions from galactic dust, CO lines, synchrotron radiation and point and extended infrared sources. The TSZ effect has a unique dependence with frequency and it can be reliably distinguished from other components using adequate techniques to reduced foreground contamination and the cosmological CMB signal (our cleaning procedure is extensively described in [72]). We will analyze only the High Frequency Instrument (HFI) data. This instrument operates at frequencies 100–857 GHz, with angular resolutions $\theta_{FWHM} \leq 10 \text{arcminutes}$. It has better angular resolution and lower instrument noise than the Low Frequency Instrument (30–70 GHz). We will measure the TSZ cluster profile at 100, 143, and 353

¹ Data are available at <http://www.cosmos.esa.int/web/planck>

Parameter	Priors
$P_c/[10^{-2} \text{ cm}^{-3} \text{ keV}]$	[0.0, 3.0]
δ	[-0.999, 1.0]
$L/[\text{Mpc}]$	[0.01, 20]
γ	[1.0, 5/3]

Table I: Parameter space explored by the MCMC

GHz channels, since after cleaning the data at 545 GHz is still dominated by residual foreground emission. In those channels, Coma pressure profile has been measured from 5 to 100 arcminutes. At 217 GHz the TSZ is greatly reduced and provides no relevant information. The details on *Planck* data processing are deferred to App. A.

V. METHODOLOGY.

To constraint extended theories of gravity using the pressure profile of the Coma cluster, we first measure the average TSZ emission ($\delta\bar{T}(\nu_k, \theta_i)/T_0$) over disc/rings out to ~ 100 arcminutes from center of the Coma cluster (see App. A). The model prediction is computed at the same apertures ($\delta\bar{T}(\mathbf{p}, \nu_k, \theta_i)/T_0$) (see Sec. III), and fit to the data. We compute the likelihood $-2 \log \mathcal{L} = \chi^2(\mathbf{p}, \nu_k)$ as

$$-2 \log \mathcal{L} = \chi^2(\mathbf{p}, \nu_k) = \sum_{i,j=0}^N \Delta\bar{T}_{ki}(\mathbf{p}) C_{ij}^{-1} \Delta\bar{T}_{kj}(\mathbf{p}), \quad (25)$$

where $\Delta\bar{T}_{ki}(\mathbf{p}) \equiv \frac{\delta\bar{T}(\mathbf{p}, \nu_k, \theta_i)}{T_0} - \frac{\delta\bar{T}(\nu_k, \theta_i)}{T_0}$, $N = 22$ is the number of data points, $\mathbf{p} = [P_c, \gamma, \delta, L]$ are the parameters of the model, ν_k denotes each *Planck* channel and C_{ij} is the correlation matrix (see eq. (A1)). When computing the likelihood we neglect the error on the CMB blackbody temperature T_0 and the uncertainty on the angular scale that corresponds to each data point since they are both negligible with respect to the error on the TSZ temperature anisotropies.

A. Monte Carlo Markov Chain sampling method

We constraint the $f(R)$ model parameters using a Monte Carlo Markov Chain (MCMC). We employ the Metropolis-Hastings [73, 74] sampling algorithm and we use the Gelman-Rubin criteria to test the mixing and convergence of our runs [75]. We run four independent chains starts at a random point of the parameter space and contains at least 40,000 steps. The step size is adapted in order to reach an optimal acceptance rate between 20% and 50% [76, 77]. If the step size is too small the acceptance rate will be too high ($\geq 50\%$) resulting in poor mixing and if the step is too large then the acceptance rate will be small ($\leq 20\%$) and the chain will converge slowly.

The parameter space explored by our MCMC is given in Table I. Intervals are chosen on physical grounds:

the central pressure P_c must be positive; in the central pixel we measure $y_C \simeq 150 \mu\text{K}$ that corresponds to $\sim 1.37 \times 10^{-2} \text{ cm}^{-3} \text{ keV}$, thus $[0.0 - 3.0] \times 10^{-2} \text{ cm}^{-3} \text{ keV}$ represents a suitable range; ICM models having the polytropic index $\gamma > 5/3$ are convectively unstable [78], therefore γ is varied between the isothermal and the adiabatic limits $\gamma = [1.0, 5/3]$; the gravitational potential diverges at $\delta = -1$ and becomes repulsive at $\delta < -1$, following [43] we set $\delta = [-0.999, 1.0]$. This range also includes $\delta = 0$ for which the Yukawa term disappears and the cluster gravitational potential is Newtonian, shallower than in the concordance model since it does not contain DM, being generated only by the baryonic component. The gravitational scale length L varies between two limiting scales: from galaxy scales [40] to the mean cluster separation scale, $L = [0.01, 20]$ Mpc. Finally, we merged the four chains and used the marginalized distributions to compute the best fit parameters and their 1σ errors bars.

VI. RESULTS AND DISCUSSION.

To test for consistency, we performed two different analyses. First, MCMC are run independently fitting separately the data at each frequency. Second we computed the joint likelihood $\mathcal{L}(\mathbf{p}) = \prod_k \mathcal{L}(\mathbf{p}, \nu_k)$. We found that the best fit parameters at the three frequencies are consistent with each other and with the results obtained from the joint distribution, indicating that our cleaning procedure does not distort the TSZ emission of the cluster and that the data at each frequency only differ in the level of the remaining foreground residuals. Due to this internal consistency hereafter we will only quote the results derived from the joint analysis.

Fig. 1 illustrates the MCMC convergence after an initial burn-in phase ($\lesssim 100$ steps). We represent the trace plot of likelihood values of the first five thousand steps of each chain. To ensure good mixing we use the Gelman-Rubin criteria requiring the ratio of the variances in the target distribution to be $\mathcal{R} < 1.03$ (see Sec. 3.2 of [79] for definitions). In our chains we found $\mathcal{R} = 1.007$.

In Fig. 2, we represent the 2D probability contours at the 68% CL (dark gray) and 95% CL (light gray) for pairs of parameters and the 1D probability distribution of each parameter. Compared with [43], the 2D contours are closed allowing us to derive new constraints on (δ, L) ; these results are summarized in Table II

The table summarizes two important results: for the first time the central amplitude of the TSZ profile in Coma cluster has been constrained in $f(R)$ gravity and $\delta \neq 0$ at the 95% CL; this latter result clearly shows that the data is compatible with $f(R)$ -gravity plus baryons, and could be interpreted as statistical evidence in favor of modified gravity and against GR plus DM. The value $L = 0$ is also ruled out at the 95% of CL. This limit corresponds to a Newtonian gravitational potential generated by a mass $M' = M/(1 + \delta)$. Since the data favors

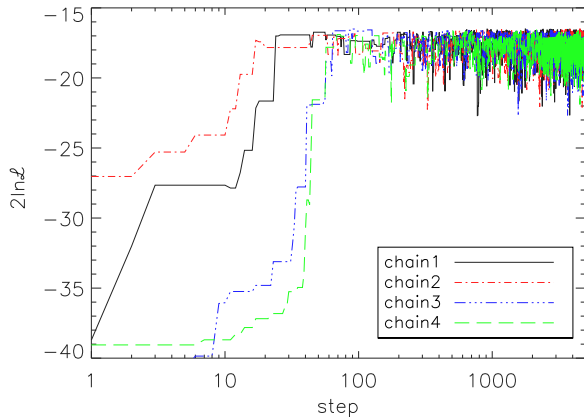


Figure 1: Trace plot of the Likelihood values of the four MCMC. Only the first 5,000 steps have been represented to better visualize the burn-in phase.

Parameter	Results
$P_c (10^{-2} \text{ cm}^{-3} \text{ keV})$	0.90 ± 0.04
δ	-0.48 ± 0.22
L (Mpc)	2.19 ± 1.02
γ	$1.44^{+0.10}_{-0.17}$

Table II: Results from the MCMC.

models with $\delta < 0$, $M' \gg M$ is analogue to the field generated by a cluster that contains a large fraction of DM distributed like the baryonic gas. To conclude, *to explain the pressure profile of the COMA cluster, either DM or a modified theory of gravity is required.* We found that the preferred value of the polytropic index is $\gamma = 1.44^{+0.10}_{-0.17}$. The best fit value is compatible at the 1.5σ level with $\gamma \sim 1.2$, the value preferred by observations and numerical simulations [80–83]. Since the polytropic index is determined by physical processes that drive the cluster collapse and its subsequent relaxation [84], our results support the idea that analytic $f(R)$ models without a dominant DM component can explain the structure of galaxy clusters as the Λ CDM model.

To illustrate the quality of the fit to the data by the model, in Fig. 3 we plot the data (diamonds) with their associated error bars and the best fit model (solid line). Panels (a-c) correspond to the three different frequencies. The χ^2 per d.o.f is given in each panel. The plot shows a slight departure from the model in the outskirts of the cluster, specially evident at 353 GHz. Since our clean patches are generated centered on the cluster, the outer parts of the cluster profile is the region most affected by foreground residuals. This is particularly true at 353 GHz where we estimate a residual of $\sim 5\mu\text{K}$ compared with $\sim 1\mu\text{K}$ at the other two frequencies. However, this departure could be due to physical reasons such as the

gas not being in hydrostatic equilibrium, departures from spherical symmetry and the presence of substructure. In order to study the impact of such phenomena one should include a non-thermal term in the pressure. For that, either N-body simulations of each specific $f(R)$ model or a scaling relation to estimate such non-thermal component are needed. Since the latter has been achieved using hydrodynamical N-body simulations in Λ CDM, its use could bias the results forcing the model to mimic the DM in the outskirts masking any effect due to the modified theory of gravity. Finally, it has been shown in [25, 26] that such contributions are negligible when, as in this work, the analysis is restricted to the intermediate regions of the cluster.

The resolution of our foreground clean maps is 10 arcminutes and the data do not probe the innermost region where shock heating, turbulence, cooling flows and other physical processes can deviate the dynamical state of the gas from hydrostatic equilibrium. Also, we did not stack the cluster profile outside $\theta > 100$ arcminutes since dust residuals dominate over the TSZ emission. To test the theory of gravity using data from the cluster core would require a good understanding of the physical phenomena to separate the physical effects associated with the dynamical state of the gas from those associated with the modified theory of gravity and an extensive study with numerical hydro-codes would be needed to compute the pressure profile. In any case, the next-generation of full sky CMB missions such as CORe/PRISM [96] will resolve the core, opening to the possibility to properly study the coupling/degeneracies between the underlying theory of gravity and the baryonic processes.

VII. CONCLUSIONS.

Cluster of galaxies have been widely used to constrain chameleon $f(R)$ models ([19, 25, 27]), the Galileon gravity model [26], the K-mouflage modification of gravity [85] and $f(\chi)$ gravity models [86]. We have constrained a particular class of ETGs using the TSZ temperature anisotropies due to the Coma cluster. With respect to previous works, in our model we introduce a Yukawa-like correction to the Newtonian potential in the weak field limit of an analytic $f(R)$ model. To test such model, we have produced foreground cleaned patches of the Coma cluster from the 2013 data release of *Planck* Nominal maps. The measured TSZ profile was used to constrain the model parameters using an MCMC algorithm assuming that the gas was in hydrostatic equilibrium within the potential well and the physical state of the ICM was well described by a polytropic equation of state. The correctness of these hypotheses can only be tested using hydrodynamical simulations. However since ETGs have extra degrees of freedom compared to GR, each specific Lagrangian would require its own set of simulations. Lacking this information we could not study the effect of a possible departure of hydrostatic equilibrium as well

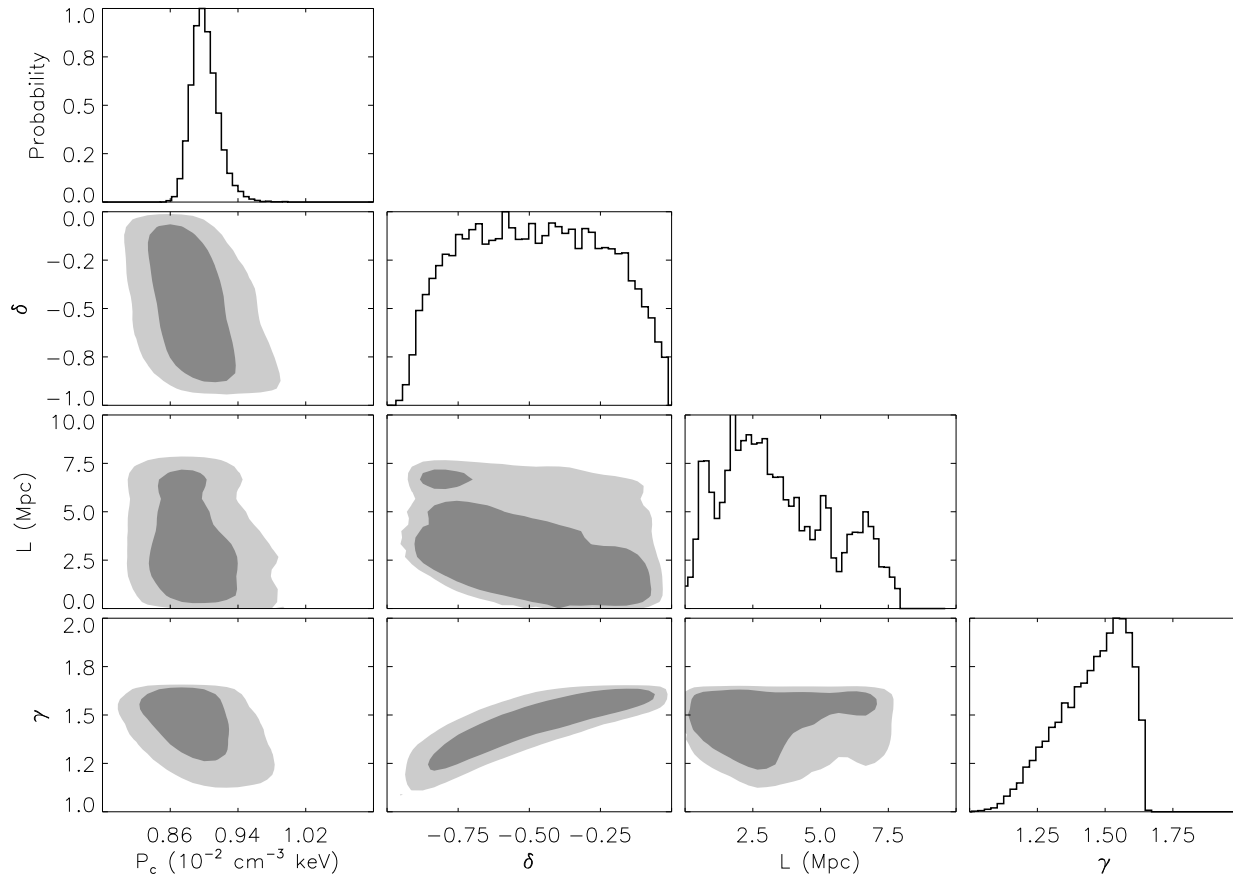


Figure 2: 2D marginalized contours of the model parameters (P_c, δ, L, γ) obtained from the MCMC analysis. For each pair of parameters the 68% (dark gray) and 95% CL (light gray) are shown. In each row, the right panels represent the marginalized likelihood distributions.

as possible degeneracies between baryonic processes and the underlying theory of gravity.

Even though we have studied a single cluster, the marginalized likelihood functions displayed closed contours. This analysis provided a more sensitive statistic and allows us to improved our earlier results [43]. The best fit values of the model parameters are summarized in Table II. We confirm that the value $\delta \simeq 0$ and $L = 0$ are ruled at the 95% CL, demonstrating that the dynamical state of the Coma cluster gas is either in equilibrium of the gravitational field of a DM halo or the gravitational field is modified by a Yukawa-type correction. This latter idea finds additional support since the best fit value of the polytropic index $\gamma = 1.44^{+0.10}_{-0.17}$ is compatible with

observations and numerical simulations.

VIII. ACKNOWLEDGMENTS

IDM was supported by University of the Basque Country UPV/EHU under the program "Convocatoria de contratación para la especialización de personal investigador doctor en la UPV/EHU 2015", and by the Spanish Ministerio de Economía y Competitividad through grant FIS2014-57956-P (comprising FEDER funds). IDM warmly thank F. Atrio-Barandela and M. de Laurentis for useful comments and discussions.

[1] Astier, P., Guy, J., Regnault, N., Pain, R., Aubourg, E., Balam, D., Basa, S., Carlberg, R. G., Fabbro, S., Fouchez, D., et al., *A&A*, **447**, 31 (2006)

[2] Blake, Chris; Kazin, Eyal A.; Beutler, F., Davis, T. M., Parkinson, D., Brough, S., Colless, M., Contreras, C., Couch, W., Croom, S., et al., *MNRAS*, **418**, 1707 (2011)

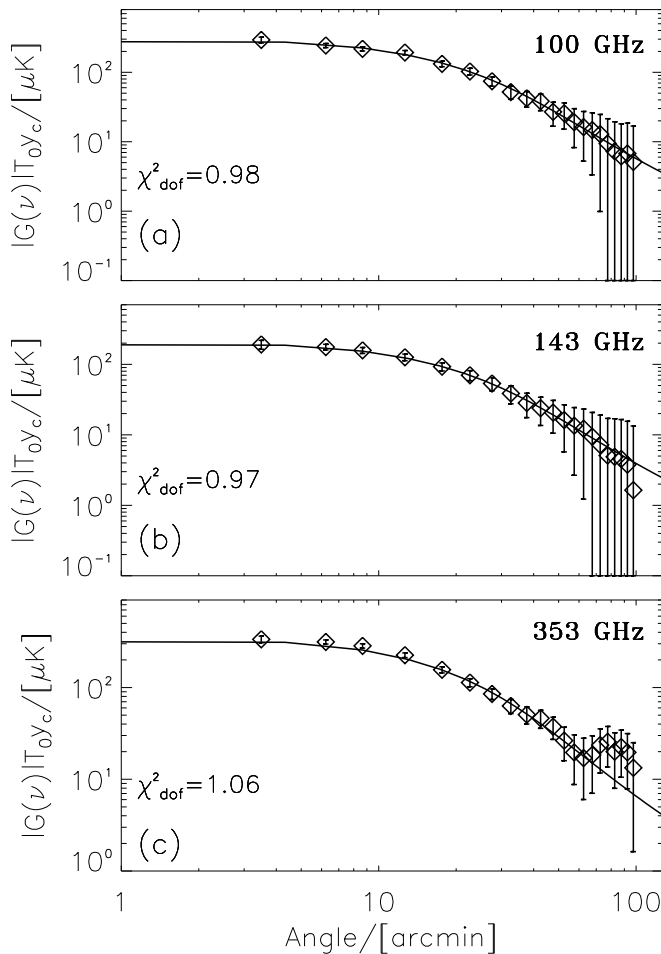


Figure 3: Predicted and measured TSZ profile of the Coma cluster at different frequencies. For each channel, the $f(R)$ best fit model has been convolved with the antenna beam.

- [3] Clocchiatti, A., Schmidt, B. P., Filippenko, A.V., Challis, P., Coil, A. L., Covarrubias, R., Diercks, A., Garnavich, P., Germany, L., Gilliland, R., et al., *ApJ*, **642**, 1 (2006)
- [4] Hinshaw, G., Larson, D., Komatsu, E., Spergel, D. N., Bennett, C. L., Dunkley, J., Nolte, M. R., Halpern, M., Hill, R. S., Odegard, N., et al., *ApJS*, **208**, 19H (2013)
- [5] Planck Collaboration. Planck 2015 results. XIII. Cosmological parameters. *A&A*, submitted. arXiv:1502.01589v2 (2015)
- [6] Riess, A.G., Strolger, L.G., Tonry, J., Casertano, S., Ferguson, H.C., Mobasher, B., Challis, P., Filippenko, A. V., Jha, S., Li, W., *ApJ*, **607**, 655 (2004)
- [7] Carroll, S.M., Duvvuri, V., Trodden, M. & Turner, M.S., *Phys Rev D*, **70**, 043528 (2004)
- [8] Sotiriou, T.P. & Faroni, V., *Rev Mod Phys*, **82**, 451 (2010)
- [9] De Felice, A. & Tsujikawa, S., *Living Rev Rel*, **13**, 3 (2013)
- [10] Nojiri, S., Odintsov, S.D., *Int. J. Geom. Meth. Mod. Phys.*, **4**, 115 (2007)
- [11] Nojiri, S., Odintsov, S.D., *Phys. Rept.*, **505**, 59 (2011)
- [12] Capozziello, S., De Laurentis, M., *Phys. Rept.*, **509**, 167 (2011)
- [13] de Martino, I., De Laurentis, M., Capozziello, S., *Universe*, **1**, 123 (2015)
- [14] Khoury, J., & Weltman, A., *Phys. Rev. D*, **69**, 044026 (2004)
- [15] Mota, D.F., & Barrow, J.D., *Phys. Lett. B*, **581**, 141 (2004)
- [16] Ferraro, S., Schimdt, F., Hu, W., *Phys Rev D*, **83**, 063503 (2011)
- [17] Hu, W. & Sawicki, I., *Phys Rev D*, **76**, 064004 (2007)
- [18] Hu, W. & Sawicki, I., *Phys Rev D*, **76**, 104043 (2007)
- [19] Li, B., He, J.-H., Gao, L., *MNRAS*, **456**, 146 (2015)
- [20] Lima, N.A. & Liddle, A.R., *Phys Rev D*, **88**, 043521 (2013)
- [21] Sawicki, I. & Hu, W., *Phys Rev D*, **75**, 127502 (2007)
- [22] Schimdt, F., Vikhlinin A., Hu, W., *Phys. Rev. D*, **80**, 083505 (2009)
- [23] Song, Y.S., Hu, W. & Sawicki, I., *Phys Rev D*, **75**, 044004 (2007)
- [24] Arnold, C., Puchwein, E. & Springer, V., *MNRAS*, **440**, 833 (2014)
- [25] Terukina, A., Lombriser, L., Yamamoto, K., Bacon, D., Koyama, K., & Nichol, R. C., *JCAP*, **04**, 013 (2014)
- [26] Terukina, A., Yamamoto, K., Okabe, N., Matsushita, K., Sasaki, T., *JCAP*, **10**, 64 (2015)
- [27] Wilcox, H., Bacon, D., Nichol, R. C., Rooney, P. J., Terukina, A., Romer, A. K., Koyama, K., Zhao, G.-B., Hood, R., Mann, R. G. et al., *MNRAS*, **452**, 1171 (2015)
- [28] Capozziello, S. & Faraoni, V., *Beyond Einstein Gravity: A Survey of gravitational Theories for Cosmology and Astrophysics*. Springer, Heidelberg (2010)
- [29] Capozziello, S. Stabile, A. & Troisi, A., *Modern Physics Letters A*, **24**, 09 (2009)
- [30] Capozziello, S. & De Laurentis, M., *Ann. Phys.*, **524**, 1 (2012)
- [31] Quandt, I. & Schmidt, H. J., *Astron. Nachr.*, **312**, **97** (1991)
- [32] Allemandi, G., Francaviglia, M., Ruggiero, M. and Tartaglia A., *Gen. Rel. Grav.*, **37**, 1891 (2005)
- [33] Berry, C. P. L. & Gair, J. R., *Phys Rev D*, **83**, 104022 (2011)
- [34] Capozziello, S. & Troisi, A., *Phys Rev D*, **72**, 044022 (2005)
- [35] Capozziello, S. & Tsujikawa, S., *Phys Rev D*, **77**, 107501 (2008)
- [36] Capozziello, S., De Laurentis, M., De Martino, I., Formisano, M., Odintsov, S. D., *Phys Rev D*, **85**, 044022 (2012)
- [37] De Laurentis, M., De Martino, I., *MNRAS*, **43**, 741 (2013)
- [38] De Laurentis, M., De Martino, I., *Int. J. Geom. Methods Mod. Phys.* **12**, 1550040 (2015)
- [39] Cardone, V. F. & Capozziello, S., *MNRAS*, **414**, 1301 (2011)
- [40] Napolitano, N. R., Capozziello, S., Romanowsky, A. J., Capaccioli, M. & Tortora, C., *ApJ*, **748**, 87 (2012)
- [41] Capozziello, S., De Filippis, E. & Salzano, V., *MNRAS*, **394**, 947 (2009)
- [42] Sunyaev, R. A., & Zeldovich, Y. B., *Comments on Astrophys. Space Phys.*, **4**, 173 (1972)
- [43] De Martino, I.; De Laurentis, M.; Atrio-Barandela, F.; Capozziello, S., *MNRAS*, **442**, 921 (2014)
- [44] The Veritas Collaboration, *ApJ*, **757**, 123 (2012)
- [45] Stelle, K., *Gen. Relat. Grav.*, **9**, 343 (1978)
- [46] Weinberg, S., *Gravitation and Cosmology*. New

- York, Wiley (1972)
- [47] Eingorn, M., & Zhuk, A., Phys. Rev. D, **84**, 024023 (2011)
- [48] Capozziello, S., Nojiri, S. and Odintsov, S.D., Phys. Lett.B 634, **93** (2006)
- [49] Capozziello, S., Nojiri, S., Odintsov, S.D. and Troisi, A., Phys. Lett.B, **639**, 135 (2006)
- [50] Nojiri, S., Odintsov, S.D., Phys. Rev. D, **74**, 086005 (2006)
- [51] Capozziello, S. Stabile, A. & Troisi, A., Mod. Phys. Lett.A **21**, 2291 (2006)
- [52] Sotiriou, T.P., Class. Quant. Grav. **23**, 5117 (2006)
- [53] Capozziello, S., Corda, C., & de Laurentis, M., Physics Letters B, **669**, 255 (2008)
- [54] Sunyaev, R. A. & Zeldovich, Y. B., MNRAS, **190**, 413 (1980)
- [55] Fixsen, D.J., ApJ, **707**, 916 (2009)
- [56] Vikhlinin, A., Kravtsov, A., Forman, W., et al., ApJ, **640**, 691 (2006)
- [57] Itoh, N., Kohyama, Y. & Nozawa, S., ApJ, **502**, 7 (1998)
- [58] Nozawa, S., Itoh, N. & Kohyama, Y., ApJ, **508**, 17 (1998)
- [59] Nozawa, S., Itoh, N., Suda, Y. & Ohhata, Y., Nuovo Cimento, **121**, 487 (2006)
- [60] Gorski, K., Hivon, E., Banday, A., Wandelt, B.D., Hansen, F.K., Reinecke, M. & Bartelmann, M., ApJ, **622**, 759 (2005)
- [61] Reiprich, T. H.; Böhringer, H., ApJ, **567**, 716 (2002)
- [62] Planck Collaboration. Planck Intermediate Results X: Physics of the hot gas in the Coma cluster, A&A, **554**, 140 (2013)
- [63] Simionescu, A., Werner, N., Urban, O., et al. ApJ, **775**, 4 (2013)
- [64] Sato, T., Matsushita, K., Ota, N., Sato, K., Nakazawa, K., Sarazin, C.L., Publ. Astron. Soc. Jpn. **63** (2011) 991
- [65] Neumann, D.M., Lumb, D.H., Pratt, G.W. and Briel, U.G. A&A **400**, 811, (2003)
- [66] Sanders, J.S., et al., Science, **341**, 6152 (2013)
- [67] Churazov, E., Vikhlinin, A., Zhuravleva, I., Schekochihin, A., Parrish, I., Sunyaev, R., Forman, W., Böhringer, H., Randall, S., MNRAS, **421**, 1123, (2012)
- [68] Snowden, S. L., Mushotzky, R. F., Kuntz, K. D., Davis, D. S. A&A **478** (2008) 615.
- [69] Wik, D.R. et al., ApJ **696**, 1700, (2009).
- [70] Gastaldello, F. et al., ApJ, **800**, 139, (2015)
- [71] Fusco-Femiano, R., Lapi, A., Cavaliere, A., ApJ, **763**, 1, (2013)
- [72] de Martino, I., Génova-Santos, R., Atrio-Barandela, F., Ebeling, H., Kashlinsky, A., Kocevski, D. & Martins, C.J.A.P., ApJ, **808**, 128 (2015)
- [73] Hastings, W.K., Biometrika, **57**, 97 (1970)
- [74] Metropolis, N., et al., J. Chem., Phys., **21**, 1087 (1953)
- [75] Gelman, A., and Rubin, D.B., Statist. Sci., **7**, 457 (1992)
- [76] Gelman, A., Roberts, G. O., Gilks, W. R., Bayesian statistics, **5**, 599 (1996)
- [77] Roberts, G. O., Gelman, A., Gilks, W. R., Ann. Appl. Probab., **7**, no. 1, 110 (1997)
- [78] Sarazin, C.L. (1988), "X-ray Emission from Clusters of Galaxies", Cambridge Astrophysics Series, Cambridge University Press.
- [79] Verde, L., Peiris, H. V., Spergel, D. N., Nolta, M. R., Bennett, C. L., Halpern, M., Hinshaw, G., Jarosik, N., Kogut, A., Limon, M., et al., ApJS, **148**, 195 (2003)
- [80] Ascasibar, Y.; Sevilla, R.; Yepes, G.; Müller, V.; Gottlöber, S., MNRAS, **371**, 193 (2006)
- [81] Bode, P., Ostriker, J. P., Vikhlinin, A., ApJ, **700**, 989 (2009)
- [82] Capelo, P. R.; Coppi, P. S.; Natarajan, P., MNRAS, **422**, 686C (2012)
- [83] Ostriker, J. P., Bode, P., & Babul, A., ApJ, **634**, 964 (2005)
- [84] Bertschinger, E., ApJS, **58**, 39 (1985)
- [85] Brax, P., Rizzo, L.A., and Valageas, P., Phys. Rev. D, **92**, 043519 (2015)
- [86] Bernal, T., López-Corona, O., Mendoza, S., arXiv:1505.00037 (2015)
- [87] Bobin, J., Sureau, F., Paykari, P., Rassat, A., Basak, S., & Starck, J.-L., A&A, **553**, L4 (2013)
- [88] Bobin, J., Sureau, F., Starck, J.-L., Rassat, A. & Paykari, P., A&A, **563**, 105 (2014)
- [89] Planck Collaboration, "Planck 2013 results. XIII. Galactic CO emission", A&A, **571**, 13 (2014)
- [90] Planck Collaboration, "Planck 2013 results. XXVIII. The Planck Catalogue of Compact Sources", A&A, **571**, 28 (2014)
- [91] Planck Collaboration, "Planck 2013 results. XXIX. The Planck catalogue of Sunyaev-Zeldovich sources", A&A, **571**, 29 (2014)
- [92] Planck Collaboration, "Planck 2013 results. XI. All-sky model of thermal dust emission", A&A, **571**, A11 (2014)
- [93] Planck Collaboration, "Planck 2013 results. XII. Component separation", A&A, **571**, 12 (2014)
- [94] Diego, J.M., Vielva, P., Martínez-Gonzalez, E., Silk, J. & Sanz, J.L., MNRAS, **336**, 1351 (2002)
- [95] Piffaretti R., Arnaud M., Pratt G.W., Pointecouteau E., Melin J.-B., A&A, **534**, 109 (2011)
- [96] PRISM Collaboration; André P. et al., JCAP, **1402**, 006 (2014)

Appendix A

In this Appendix we briefly describe the method used to clean *Planck* 2013 Nominal maps and the errors on the measured TSZ profile. More details are given in [72]. Briefly,

- all *Planck* channels are downgraded to a common 10 arcmin resolution assuming a Gaussian beam for;
- at each frequency, the cosmological CMB and KSZ signals are removed by subtracting the LGMCA CMB template of [87, 88];
- CO emission at 100 and 217 GHz is removed by subtracting the CO Type 2 maps provided by the Planck Collaboration [89],
- point sources and foreground residuals close to the Galactic Plane are excised with the PCCS-SZ-Union mask [90, 91];
- finally, the thermal dust emission is removed using the 857 GHz channel as a dust-template [92, 93], following the method described in [94].

At each frequency, from 100 GHz to 545 GHz, our

cleaning method provides foreground cleaned patches $\mathcal{P}(\nu, x)$ centered on the position x of the selected cluster from where we can measure the TSZ temperature fluctuations ($\delta\bar{T}/T_0$) at the cluster position. In Fig. 4 we show the patch around the Coma cluster to illustrate how effectively our cleaning procedure removes foregrounds. Temperatures are given in μK . The top row corresponds to the original *Planck* Nominal data and the bottom row to foreground cleaned maps. The Nominal patches are dominated by the intrinsic CMB temperature fluctuations, while in the foreground clean maps the TSZ signal dominates. The signal is negative at 100 and 143 GHz, zero at 217 and positive at 353 GHz, as expected. At 545 GHz is dominated by dust residuals and, together with 217 GHz that corresponds to the TSZ null, they will not be included in our analysis.

The pressure profile is constructed by taking averages on the central disc of radius 5 arcminutes and on rings of 5 arcminutes width out to 100 arcminutes. The angular scale associated to each temperature average is the mean angular distance to the center of the cluster of all pixels

within the disc or ring. The dispersion around the mean ranges from a minimum of ~ 0.5 arcminutes in the central 15 arcminutes to a maximum of ~ 1.5 arcmin. To compute the error on the measured TSZ anisotropies, we place the cluster at 1,000 random positions in the sky. The patch is cleaned as described before and the mean on the central 5 arcmin disc and rings is evaluated. To avoid overlapping with real clusters, we mask an area of one degree radius around all clusters in the [95] catalog. We repeat the procedure and compute the correlation matrix (C_{ij}) between different bins (θ_i) averaging over all random positions

$$C_{ij}(\nu_k) = \frac{\langle [\delta\bar{T}(\nu_k, \theta_i) - \mu(\nu_k, \theta_i)][\delta\bar{T}(\nu_k, \theta_j) - \mu(\nu_k, \theta_j)] \rangle}{\sigma(\nu_k, \theta_i)\sigma(\nu_k, \theta_j)}, \quad (\text{A1})$$

where $\mu(\nu_k, \theta_i) = \langle \delta\bar{T}(\nu_k, \theta_i) \rangle$, and $\sigma(\nu_k, \theta_i) = \langle [\delta\bar{T}(\nu_k, \theta_i) - \mu(\nu_k, \theta_i)]^2 \rangle^{1/2}$. The error bars on the profile of the Coma cluster are the square root of the diagonal elements of the correlation matrix.

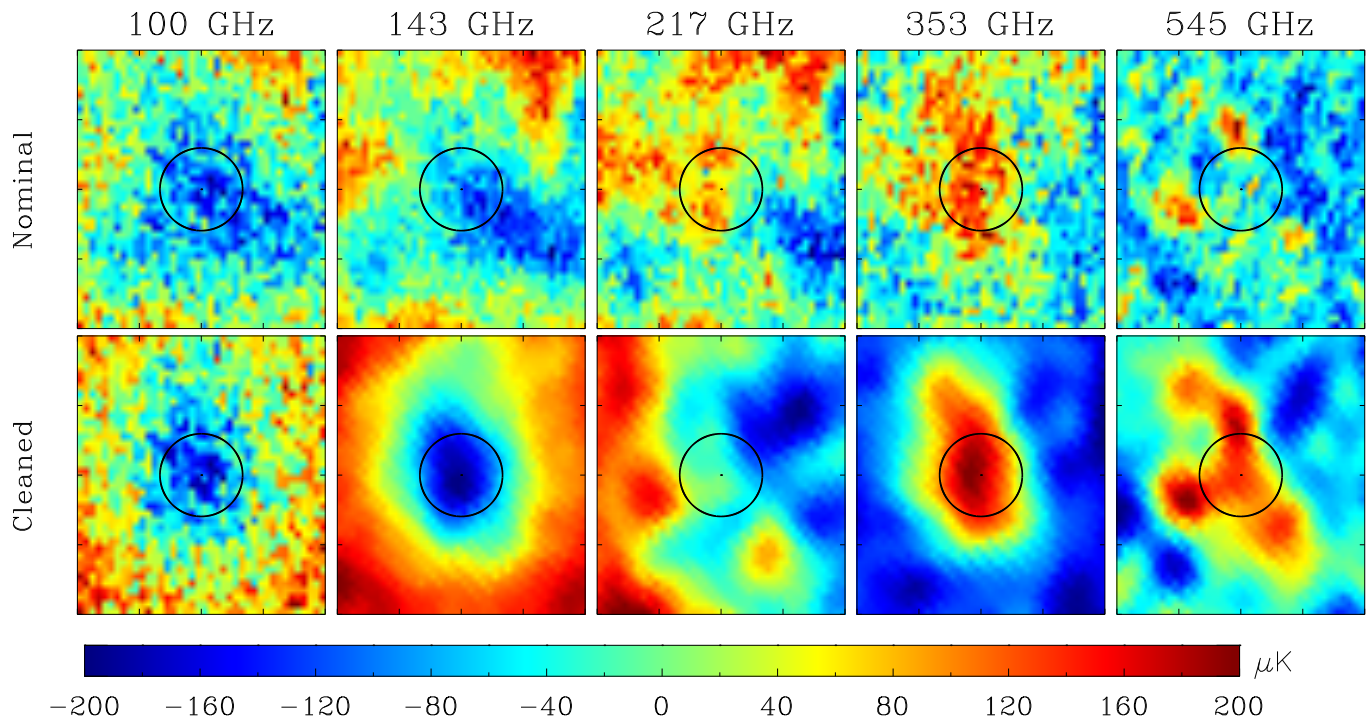


Figure 4: First and second rows: *Planck* Nominal and foreground cleaned patches centered at the position of A1656 (Coma cluster) at 100-545 GHz. Patches are $2^\circ \times 2^\circ$.